ELSEVIER

Surface Science 387 (1997) 69–77

surface science

Force microscopy of cleaved and electron-irradiated $CaF_2(111)$ surfaces in ultra-high vacuum

R. Bennewitz, M. Reichling *, E. Matthias

Freie Universität Berlin, Fachbereich Physik, Arnimallee 14, 14195 Berlin, Germany

Received 24 January 1997; received in revised form 2 April 1997

Abstract

We present scanning force micrographs of as-cleaved and electron-irradiated $CaF_2(111)$ surfaces taken in ultra-high vacuum at room temperature. Among the forces acting on the tip, the electrostatic force was found to make an important contribution. This allows us to study the ionic conductivity of the crystals. Freshly cleaved surfaces can be imaged in contact mode with high-resolution exhibiting the hexagonal structure of the (111) surface. For electron-irradiated surfaces, noncontact mode is required for imaging radiation-induced stoichiometric changes. Strong adhesive forces between the tip and metal-enriched areas are found to be a severe obstacle for contact mode imaging. Weak irradiation with 850 eV electrons results in the formation of 10 nm-wide holes with surrounding elevations as the first stages of metallization. © 1997 Elsevier Science B.V.

Keywords: Atomic force microscopy; Calcium fluoride; Electron bombardment; Halides; Insulating surfaces; Radiation damage; Surface defects

1. Introduction

Low-energy electron irradiation of CaF_2 results in formation of Ca colloids in the bulk and at the surface [1]. While bulk colloids can best be investigated by optical transmission spectroscopy, scanning force microscopy (SFM) [2] is the adequate tool for studying surface colloids. Previously, we reported on imaging the topography of metallized surfaces by SFM in contact mode in air after removal of the irradiated crystals from the ultra-high vacuum (UHV) chamber [3]. It was found that at low electron dosages circularly shaped metal colloids emerge at the surface originating from diffusion of F-centers from the bulk. Higher electron dosages produce a strong inhomogeneous metallization of the surface and tend to form larger but irregular aggregates. From these measurements two conclusions should be remembered: one is that metallization dynamics takes place during electron irradiation. The other is that exposing the crystals to air only oxidized colloids can be imaged, and the force between tip and metal aggregate is altered, compared with an unoxidized metal surface.

In this contribution, we present results of scanning force microscopy in UHV of both CaF_2 surfaces freshly cleaved in UHV, and those irradiated with electrons after cleaving. In contrast to SFM in air, in UHV contact mode during scanning, the tip tends to stick to metal colloids, which seriously impedes the imaging process. Therefore, we utilized the noncontact mode [2], which not

* Corresponding author.
E-mail: reichling@matth1.physik.fu-berlin.de

PII S0039-6028(97)00268-9

only circumvents sticking, but may also provide resolution on the atomic scale [4]. We will discuss the various types of forces between tip and surface and compare their role when scanning in air or in UHV. The electrostatic force between tip and surface turns out to be of major importance for investigating surface topographies of ionic crystals and also offers the advantage to determine the ionic conductivity of the crystal at room temperature.

2. Surfaces cleaved in UHV

CaF_2 crystals of optical quality (Karl Korth Company, Kiel) were cleaved along the (111)-plane in UHV by a light stroke with a knife blade made from hardened steel. After cleavage, crystals were typically 5 mm thick and were transferred to a commercial UHV-SFM (Omicron, Taunusstein) in the same UHV-chamber. Surfaces were scanned at room temperature with tips made from n-type silicon (Nanosensors, Wetzlar). Fig. 1 displays the topography of a CaF_2(111) surface cleaved and imaged in UHV, recorded in noncontact mode. The image exhibits atomically flat terraces with a typical extension of 100 nm and steps 0.34 nm in height, corresponding to one F–Ca–F layer in the (111) cleavage plane. Most of the steps form a zig-zag structure oriented along major crystal directions, very similar to images obtained in air [5]. However, occasionally some terraces are of very small width and form needle-like structures, as shown in Fig. 2. The reason for such different appearance is not clear. Generally, the density of steps and their orientation varies especially in the neighbourhood of macroscopic cleavage steps.

An attempt was made to explore the limits of resolution for contact mode imaging on atomically flat terraces. For this type of measurement the tip was drawn back in such a way that the contact area between tip and surface was minimized without breaking contact. A typical example is shown in Fig. 3(a). Here, we recorded the force modulation during scanning at constant height above a terrace and can resolve atomic periodicity with a lattice constant of the (111) surface, as displayed for comparison in Fig. 3(b). It is known from measurements on NaF surfaces [6] that the atomic periodicity disappears around steps since the contact area between tip and surface in contact mode is larger than atomic dimensions. For such measurements the contact area was estimated to be about 1 nm^2. It is commonly assumed that such large contact area prevents images with atomic periodicity to reveal atomic size defects. In Fig. 3(a) we indeed see a few irregularities at some

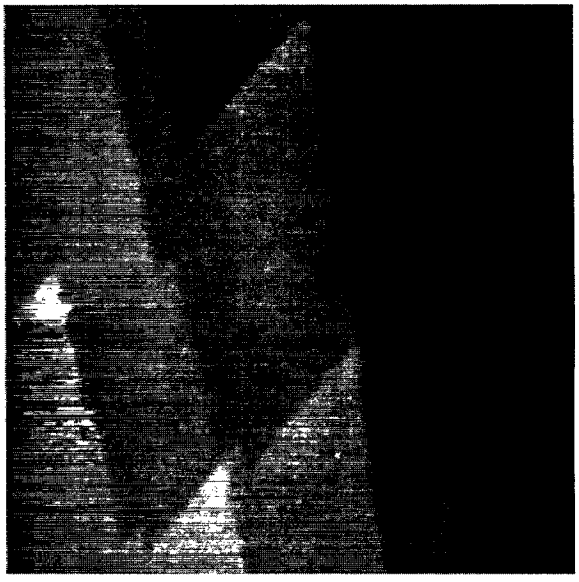

Fig. 1. Surface topography of CaF_2(111) cleaved and imaged in UHV, recorded in noncontact mode. The frame size is 150×150 nm^2. The steps are 0.34 nm high, corresponding to one F–Ca–F layer.

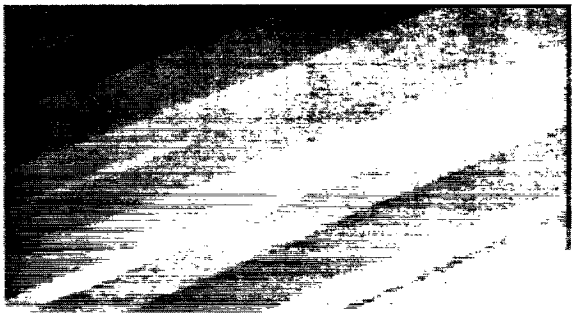

Fig. 2. Noncontact micrograph taken at another site of the surface shown in Fig. 1. The frame size is 500×270 nm^2. Here, needle-like structures are formed by atomically flat terraces. The step height is identical to that in Fig. 1.

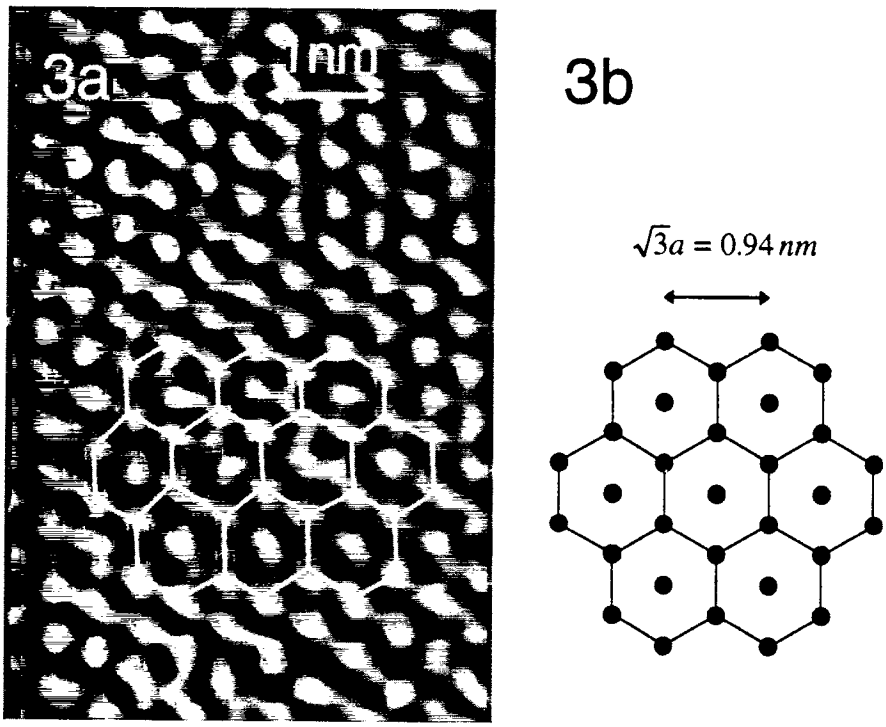

Fig. 3. (a) Normal force image recorded in constant-height mode on a (111) terrace of a CaF_2 surface cleaved in UHV. Since the signal of about 10^{-10} N was at the detection limit, the data have been filtered for better visualization of the atomic periodicity. The hexagons resemble the periodicity of the (111) surface and serve to identify irregularities. (b) Pattern of the upper anion positions in the (111) plane.

locations indicated by hexagons in form of two atomic size features where only one is expected. These features cannot be reproduced by repetitive scanning. Hence, at present it cannot be concluded that these deviations are dimer-type surface defects. Similar irregularities have been observed for LiF imaged in UHV [7] and for NaCl imaged in air [8]. It should also be remembered that modeling of contact imaging of ionic surfaces has shown [9] that an apparent atomic periodicity may not necessarily correspond to positions of surface ions and, furthermore, that the scanning process can induce major displacements of ions.

3. Contact mode imaging of electron-irradiated surfaces

In order to study colloid formation after electron bombardment, surfaces cleaved in UHV were subsequently irradiated for 7 min with 0.6 μA of 850 eV electrons. The area of the irradiated spot was 2 mm^2. During irradiation, the crystal was heated to 150°C. After irradiation, the sample was cooled to room temperature for about 100 min and transferred to the SFM. While there is no problem with contact mode imaging of Ca colloids at a CaF_2 surface in air [3], this turned out to be most difficult in UHV. The reason is that in air, the metal clusters are covered by an oxide sheet, while in UHV the clean metal surface is exposed to the tip. Fig. 4 demonstrates stripes that appear in most images which arise from sticking of the tip to the colloids and subsequent bending of the cantilever until the tip is finally pulled off by the scanning motion. To explain this phenomenon, we suggest that the conductive tip experiences a short-range adhesive force by the colloid surface due to "metallic bonding". This type of force has been described to become much stronger than van der

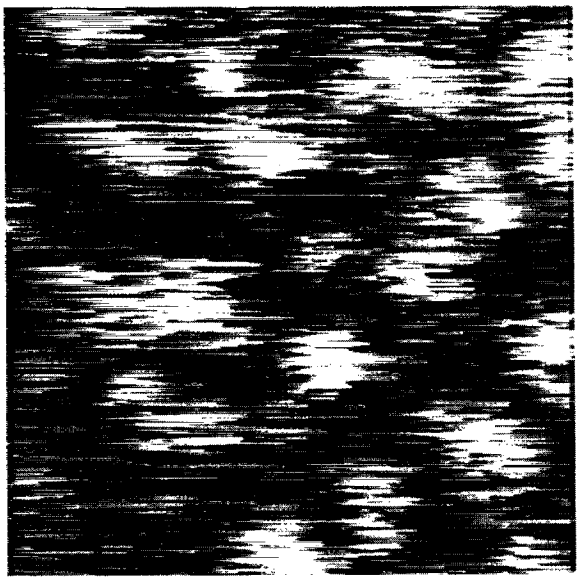

Fig. 4. Contact mode image of a surface metallized by electron irradiation for 7 min with 4 μA current. Imaging is forfeited by sticking of the tip to the irradiated surface. The frame size is $2 \times 2\ \mu m^2$.

Waals forces for tip–surface distances below 1 Å [10]. When imaging in air, on the other hand, sticking of the tip to colloids is much less likely for two reasons. First, the surface of colloids is oxidized and cannot experience metallic bonding which is based on the interaction of conduction band electrons. Second, the surface is covered by a thin water film from ambient humidity [11] that has been reported to act as an elastic lubricant [8] by diminishing the van der Waals force between tip and surface by a factor of 10 compared with UHV-SFM [12]. The limited lateral resolution and the adhesion problems encountered during colloid imaging have been major reasons for dismissing contact mode imaging for further investigations of radiation modified ionic surfaces. Hence, all measurements presented below have been carried out in noncontact mode.

4. Electrostatic forces

In noncontact mode, van der Waals forces are utilized to derive topographic information for insulator surfaces [2]. However, this interaction is small and easily dominated by stronger forces like the localized electrostatic attraction due to a trapped charge. To investigate the nature of these forces in some detail, we operated the SFM in noncontact mode and recorded the cantilever eigenfrequency as a function of the tip–surface distance (Fig. 5) and of an applied bias voltage (Fig. 6). The cantilever was excited to oscillate at its eigenfrequency with constant amplitude. The shift of the eigenfrequency is in first approximation

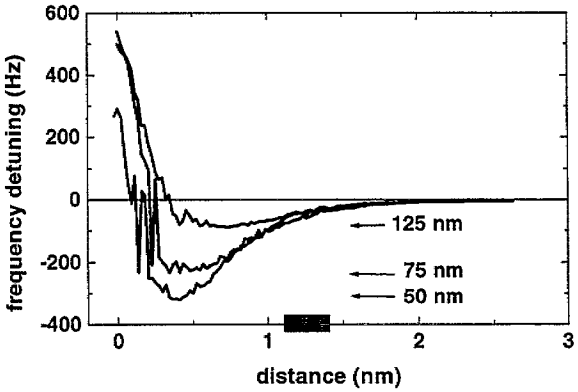

Fig. 5. Detuning of the cantilever eigenfrequency when approaching the surface with the tip. The curves are taken using different oscillation amplitudes indicated by arrows pointing to their respective minima. The shaded bar marks the range used for feedback control.

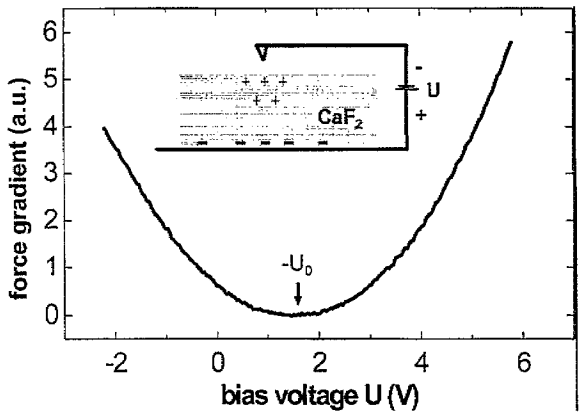

Fig. 6. Force gradient as a function of the bias voltage applied to the sample rear side. The tip was at a fixed distance from the surface in the range indicated by the bar in Fig. 5. A constant offset has been subtracted, which is equivalent to neglecting forces which do not change with bias voltage.

a linear function of the force gradient acting on the tip during oscillation [2]. Fig. 5 shows frequency shifts versus distance curves for three oscillation amplitudes typically used in our imaging experiments. The range marked by a gray bar is usually chosen for feedback control. In principle, a better lateral resolution can be achieved the closer the tip comes to the surface. However, a closer approach to the surface leads to an instability in the oscillation and the feedback control often fails to lock, especially on stepped surfaces.[1] From the differences in the curves for different oscillation amplitudes we conclude that the first-order approximation is not appropriate to quantitatively determine force gradients close to the surface. A nonlinear theory for the oscillation should be applied since oscillations with amplitudes sufficiently small to allow linearization are difficult to stabilize. Therefore, in the force curves shown below force gradients are given in arbitrary units.

To investigate the electrostatic contribution to the total force, we measured the force gradient as function of a bias voltage U applied between tip and sample holder as shown in the inset of Fig. 6. In such an arrangement, surface charges interact with the polarizable tip and exert an attractive electrostatic force $F_{el}=c(U+U_0)^2$, where c is a constant which depends on tip shape and tip–surface distance [13]. The voltage shift U_0 was found to be -1.6 V in the measurement shown in Fig. 6. For conductive materials U_0 is usually interpreted as the work function difference between tip and surface. For insulating crystals we believe that it more generally indicates the presence of a negative charge at the dielectric surface. Such charge may result from electrons transferred from the Si-tip to defect states in the CaF_2 band gap or from charged defects at the surface. Therefore, one has to apply a compensating bias voltage between the tip and the rear side of the sample to minimize such electrostatic forces (cf. Fig. 6). The appropriate voltage differs for different tips and surfaces but is generally positive and increases for irradiated surfaces.

[1] The instability range compares to the regime II described in Ref. [4].

5. Ionic conductivity

When turning the bias voltage off, we observe a reproducible relaxation of the force gradient with time. We assume that when a bias voltage U is applied to the rear side of the sample, charged defects drift in the electric field between tip and sample holder and form a macroscopic polarization in the crystal. Since this effect is directly related to charge transport in the sample, this relaxation of the force gradient can be utilized as a sensitive probe for measuring the ionic conductivity of the crystal at room temperature, a quantity which is hard to determine by other methods. The ionic conductivity of CaF_2 is believed to be mainly caused by the mobility of F^- vacancies [14]. Besides those vacancies present in the crystal due to thermodynamic equilibrium concentration of Frenkel pairs, F^- vacancies appear as charge compensation for monovalent metal impurities or for O^{2-} impurity ions at F^- sites. The latter are easily built into the lattice during crystal growth and have been shown to significantly increase the ionic conductivity of CaF_2 [15].

For a conductivity measurement, the tip is fixed at a distance z above the surface and the feedback loop is switched off. When the bias voltage is turned off at $t=0$, the surface charge decays with a time constant τ and the change of force gradient with time is measured. The decay time τ can then be related to the conductivity σ by $\tau=\epsilon\epsilon_0/\sigma$ (ϵ dielectric constant of CaF_2, ϵ_0 vacuum permittivity) [16]. The temporal development of the electrostatic force gradient can be modeled by the function

$$\frac{\partial F_{el}}{\partial z}(t)=c(U_0+U_2-(U_2-U_1)e^{(-1/\tau)})^2, \qquad (1)$$

where U_1 and U_2 are the initial and final bias voltages. A fit to experimental data provides a value for the decay time τ.

A typical relaxation curve of the force gradient after switching the bias voltage from $U_1=4$ V to $U_2=0$ V is shown in Fig. 7. Since the force between a surface charge and a polarizable tip is always attractive, the curve passes a minimum when the surface charge vanishes. The solid line represents

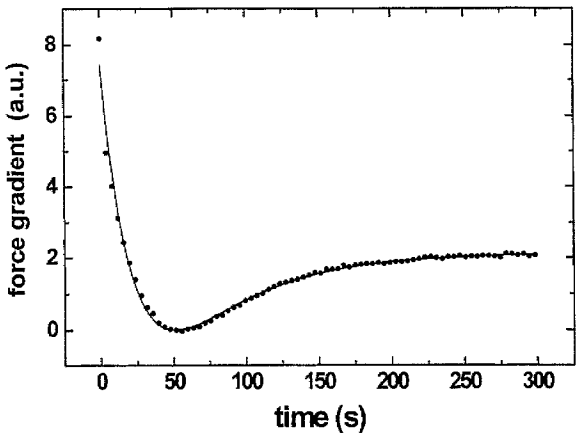

Fig. 7. Time dependence of the force gradient after switching the bias voltage from 4 to 0 V at $t=0$. The tip was at a similar distance from the surface as for the measurement shown in Fig. 6.

the best fit of the above equation to the data and yields $\tau=50$ s which converts to an ionic conductivity $\sigma=(1.2\pm0.4)\times10^{-14}\,\Omega^{-1}\,\mathrm{cm}^{-1}$. The same order of magnitude is obtained by an exponential extrapolation of high temperature data to room temperature for CaF_2 crystals slightly contaminated by O^{2-} ions [15]. It is worth mentioning that great care must be taken to have the system in stable equilibrium for this type of measurement otherwise instrumental drift may influence the result. Any interactions of external charge sources in the vacuum chamber during the conductivity measurement have been excluded by our experimental configuration; for example, switching on and off the ion gauge did not affect the relaxation.

6. Colloid formation during electron irradiation

One of the initial goals for applying force microscopy to CaF_2 surfaces was to gain a better understanding of colloid formation during electron irradiation. In our previous SFM investigation of electron-irradiated surfaces *in air*, the formation of smooth, spherical colloids was observed [3]. Therefore, it was assumed that Ca ions at the surface have been neutralized by surrounding F-centers and become mobile to aggregate and form metallic colloids. After removal of the calcium colloids by washing the surface with water holes at the surface were found. We interpreted these holes as endpoints of channels of enhanced metal diffusion from the bulk feeding surface colloid formation. Such channels could originate from F-center aggregation along dislocations [17].

In the present UHV study one striking result is that after electron irradiation conspicuous depressions appear which are very similar to the holes found below colloids in the air experiments [3], but in UHV they are not covered by metal. Instead, bright features are located eccentrically next to the holes. The upper part of Fig. 8 shows such holes formed during irradiation with electrons (850 eV energy, 0.3 $\mu A\,mm^{-2}$) for 2 min at 150°C. The holes are randomly distributed and irregularly shaped and have typically 10 nm lateral extension. In the lower part of Fig. 8, a comparison of the tip shape (10 nm radius) with the cross-section through one of the depressions shows that the depth of such holes is at least 0.3 nm, but cannot be determined definitely due to the finite size of the tip. The same holds true for the holes in the surface which had been irradiated for 10 min with the same parameters leading to an increased areal density of holes (Fig. 9). It is evident in both figures that the distribution of the holes is random and *not* gathered along cleavage steps. It can also be recognized that holes may spread across a step indicating that the mechanism of hole formation originates from the depth and is not seeded along steps. These observations coincide with our previous experiments where on electron-irradiated surfaces mostly no defect aggregation at steps was found [3], but are in contrast to the clustering of evaporated gold atoms that has been observed at steps of cleaved $CaF_2(111)$ [18]. The discrepancy may be due to different surface diffusion mobilities of calcium and gold on the dielectric surface. More likely, however, it is caused by a higher number of nucleation sites present on our electron-irradiated surface. For Si supported $CaF_2(111)$ films it has been shown that the nucleation of Fe particles on the surface can be strongly related to defects sites with a high trapping energy [19] and that electron beam modification even more stabilizes nm-sized metallic surface clusters [20]. Electron-beam-induced holes as present in Figs. 8

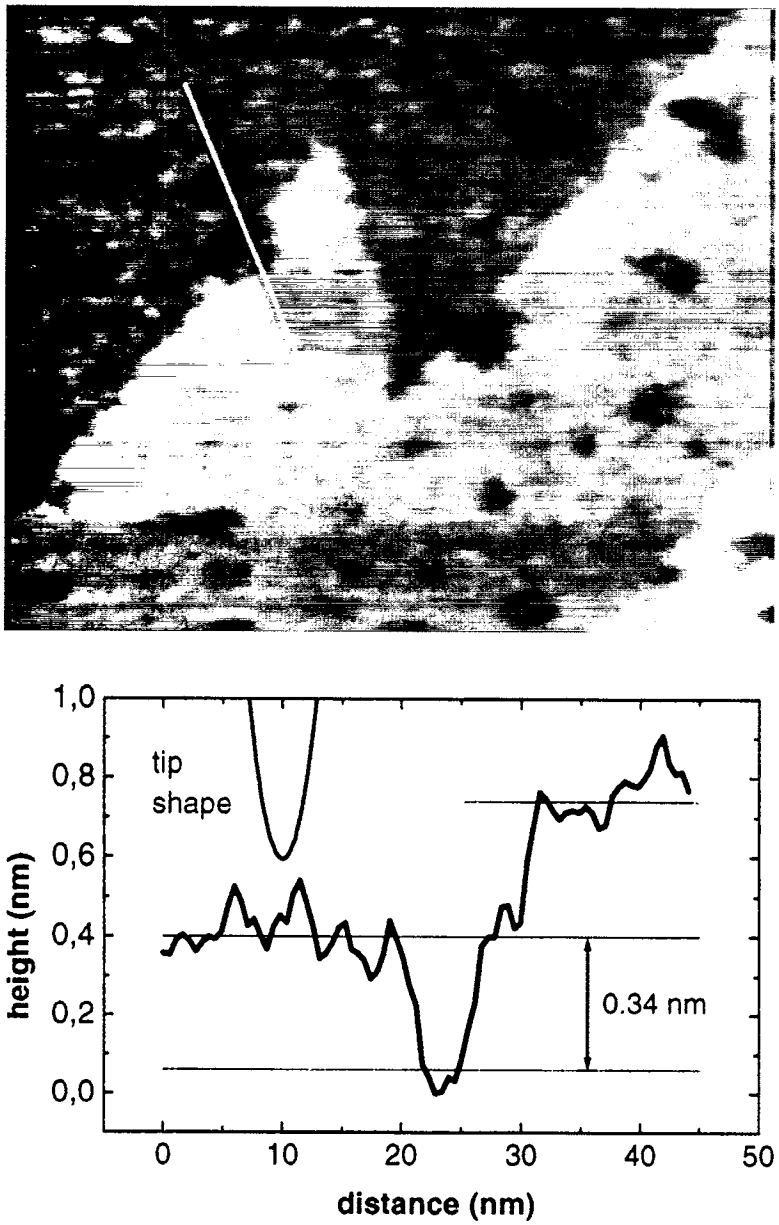

Fig. 8. Noncontact SFM image of a CaF_2 (111) surface irradiated for 2 min (115×95 nm^2). The cross-section in the lower part corresponds to the white line in the micrograph. The height of 0.34 nm corresponds to one F–Ca–F layer.

and 9 are very likely to serve as nucleation sites in that sense.

When interpreting noncontact mode images in Figs. 8 and 9 one has to keep in mind that in this mode the surface of constant force gradient is recorded, which may be determined by both, topography and force variations. For example, the bright features around the holes in Fig. 9 could represent not only topographic elevations, but also the lift off of the tip above trapped charges to keep the force gradient constant. In the latter case, the attractive interaction between tip and trapped

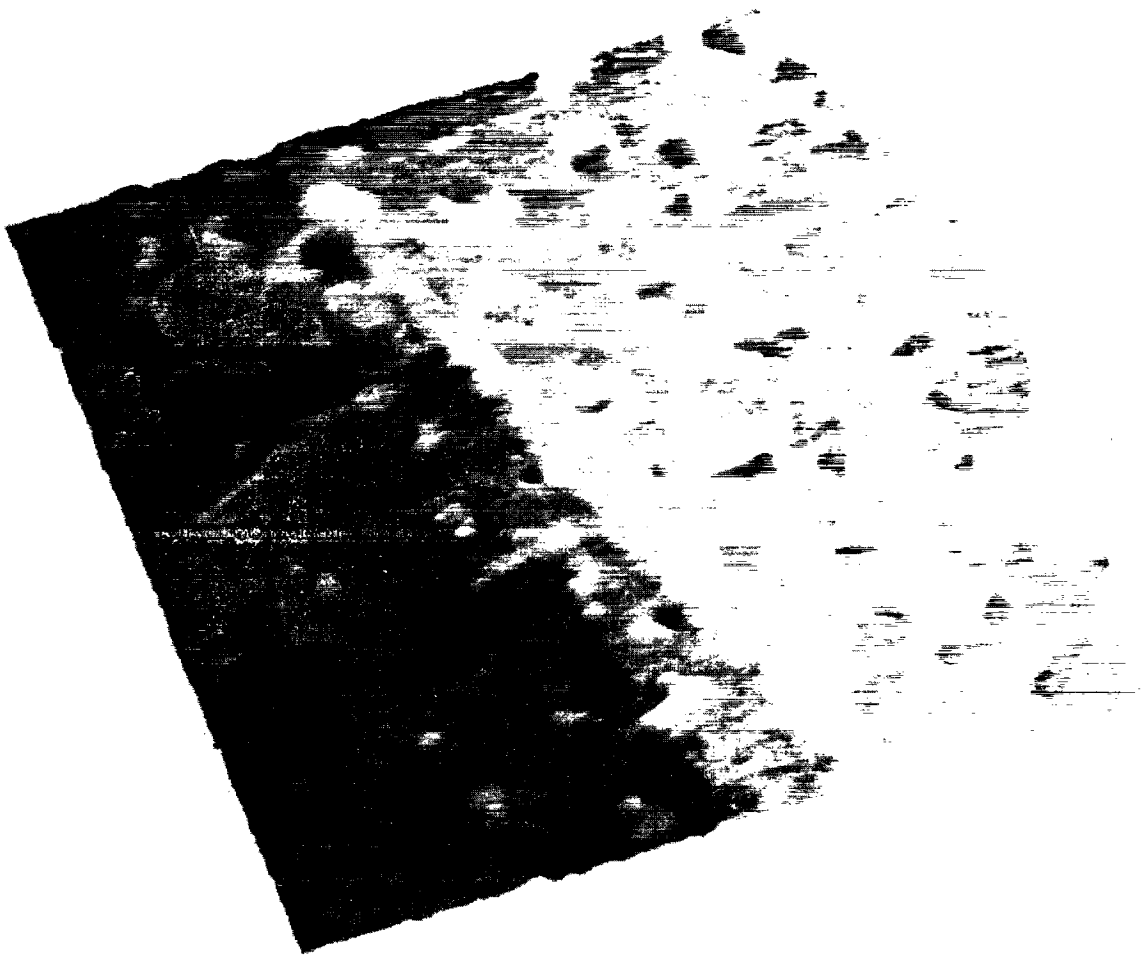

Fig. 9. Noncontact SFM image of a $CaF_2(111)$ surface irradiated for 10 min (150×150 nm^2).

charges simulates the existence of a topographic elevation. On the other hand, the holes observed are thought to really represent topographic features since no localized defect is expected to weaken the force, which is determined by the low polarizability of the unmodified CaF_2 crystal [12]. There are two possible explanations for the features observed at the rim of the holes.

(1) When they are of topographic origin, we interpret them as metallic calcium. Similar to the observations in air we assume calcium emerging from holes. In contrast to ambient atmosphere, the calcium is collected eccentrically at the rim of the holes. A quantitative comparison of hole depth and surrounding elevations is difficult since the size of the features is comparable with the tip apex. Interestingly, at each hole a certain direction seems to be preferred for the calcium aggregation. For a speculative interpretation we recall the fact that dislocations do not hit the surface perpendicularly, but at some angle [21]. If the holes form along such dislocations, an eccentric deposition of the emerging material is conceivable. On surfaces cleaved and imaged in air, the formation of spherical colloids indicates an enhanced surface mobility of metal compared with the UHV case. Possibly adsorbed water might act as lubricant at the highly defective irradiated surface.

(2) Supposing that the origin of the elevations around the holes are increased forces, we attribute

those to electrostatic attraction by trapped charges. Irradiation with electrons easily produces charged point defects like interstitial fluorine anions or vacancies. Such defects may be stabilized at the rim of the holes. This interpretation faces the problem where the material is left which is removed from the holes and which has been observed in colloidal form in air. Therefore, we favor the interpretation that the bright features in Figs. 8 and 9 are metallic calcium which is collected on the surface close to the holes. Future studies will include force spectroscopy to compare the type of interaction present at irradiation induced features and at the unmodified surface for a conclusive interpretation of noncontact images.

7. Conclusion

In summary, we have performed scanning force microscopy of $CaF_2(111)$ surfaces in UHV in contact and noncontact mode. On freshly cleaved surfaces we found atomic periodicity with irregularities on an atomic scale. Surface modifications generated by electron irradiation jam the tip and impede imaging in contact mode. The importance of electrostatic forces due to charged crystal defects was shown by recording the force gradient as a function of bias voltage applied to the sample rear side. It was found that a compensating voltage has to be applied even to bulk samples of ionic crystals to minimize the total force. The relaxation of electrostatic forces after turning off the bias voltage was utilized for measuring the ionic conductivity of the crystal at room temperature to be $\sigma=(1.2\pm0.4)\times10^{-14}\,\Omega^{-1}\,cm^{-1}$. Noncontact mode measurements allowed imaging of the early stages of electron-irradiation induced surface metallization. As in a previous study in ambient atmosphere, we found randomly distributed conspicuous holes which may have served as diffusion channels feeding the surface metallization. Elevations at the rim of such holes are tentatively interpreted as metallic calcium emerged from the holes.

Acknowledgements

We gratefully acknowledge discussions with R.M. Wilson and R.T. Williams and computer assistance by P. West. This work was supported by the Deutsche Forschunsgemeinschaft.

References

[1] R. Bennewitz, C. Günther, M. Reichling, E. Matthias, R.M. Wilson, R.T. Williams, Rad. Eff. Def. Sol. 137 (1995) 19.
[2] C.F. Quate, Surf. Sci. 299/300 (1994) 980.
[3] M. Reichling, R.M. Wilson, R. Bennewitz, E. Matthias, R.T. Williams, Surf. Sci. 366 (1996) 531.
[4] R. Lüthi, E. Meyer, M. Bammerlin, A. Baratoff, T. Lehmann, L. Howald, Ch. Gerber, H.-J. Güntherodt, Z. Phys. B100 (1996) 165.
[5] R.M. Overney, H. Haefke, E. Meyer, H.-J. Güntherodt, Surf. Sci. Lett. 277 (1992) L29.
[6] L. Howald, H. Haefke, R. Lüthi, E. Meyer, G. Gerth, H. Rudin, H.-J. Güntherodt, Phys. Rev. B49 (1994) 5651.
[7] M. Ohta, T. Konishi, Y. Sugarawa, S. Morita, M. Suzuki, Y. Enomoto, Jap. J. Appl. Phys. 32 (1993) 2980.
[8] A.L. Shluger, R.M. Wilson, R.T. Williams, Phys. Rev. B49 (1994) 4915.
[9] A.L. Shluger, R.T. Williams, A.L. Rohl, Surf. Sci. 343 (1995) 273.
[10] U. Dürig, O. Züger, D.W. Pohl, Phys. Rev. Lett. 65 (1990) 349.
[11] K. Miura, Phys. Rev. B52 (1995) 7872.
[12] J.N. Israelachvili, Intermolecular and Surface Forces, Academic Press, London, 1985.
[13] Y. Martin, D.W. Abraham, H.K. Wickramasinghe, Appl. Phys. Lett. 52 (1988) 1103.
[14] R.W. Ure, J. Chem. Phys. 26 (1957) 1363.
[15] M. Svantner, E. Mariani, Kristall und Technik 13 (1978) 1431.
[16] W.K.H. Panofsky, M. Phillips, Classical Electricity and Magnetism, 2nd ed., Addison-Wesley, Reading, 1971.
[17] C. Chassagne, D. Durand, J. Serughett, L.W. Hobbs, Phys. Stat. Sol. A41 (1977) 183.
[18] J. Viereck, W. Hoheisel, F. Träger, Surf. Sci. 340 (1995) L988.
[19] K.R. Heim, S.T. Coyle, G.G. Hembree, J.A. Venables, M.R. Scheinfein, J. Appl. Phys. 80 (1996) 1161.
[20] K.R. Heim, G.G. Hembree, M.R. Scheinfein, J. Appl. Phys. 76 (1994) 8105.
[21] A.G. Evans, P.L. Pratt, Phil. Mag. 20 (1969) 1213.